4. Beamlines

This report describes the FY2019 activities of the light source and optics of the beamlines. It includes the insertion device, front-end, optics and transport channel, and radiation shielding of SPring-8, and SACLA beamlines. In addition to routine maintenance, several component upgrades and R&D were performed. Some of these endeavors were part of the SPring-8 major upgrade.

1. Insertion device and front-end
1-1. Insertion device
(1) Maintenance
Over the past few years, insertion devices, which were installed in the storage ring more than 20 years ago, have suffered from a number of hardware issues. Affected equipment includes the power supplies to drive the steering magnet and correct the electron beam orbit during the gap motion, chillers to stabilize the temperature of the permanent magnets in in-vacuum undulators, rotary encoders to measure the magnet gap, and vacuum gauges to monitor the pressure inside the vacuum chamber. In most cases, replacement with spare parts quickly restored operations after a few hours of downtime.

Besides the issues mentioned above, BL25SU encountered a serious hardware failure of a pair of helical undulators, which have been in operation since 1997. During the regular maintenance period, a failure was found in one of the gap-driving systems of the upstream undulator. A plastic cover of the linear guide was broken, probably due to long-term radiation damage, and the bearings inside the guiding block were ejected. To avoid further mechanical damage, we decided to terminate the operation of the upstream undulator until the damaged parts have been replaced with new ones. Because the downstream undulator may have similar problems, all the linear guides for the gap motion will be replaced with new ones. The repair work will begin in summer 2020 and will be completed by the end of FY 2020. During this repair only one of the two undulators will be available for user operations.

(2) R&D toward shorter undulator periods
One R&D activity has proposed and experimentally demonstrated a new concept, which utilizes monocrystalline dysprosium (Dy) as a material for pole pieces in cryogenic undulators to shorten the undulator periods. This concept is based on the high saturated magnetic flux density of Dy (3.5 T at 4.2 K). It is about 50% higher than vanadium permendur (VP), which is a conventional material for undulator pole pieces.

To demonstrate its performance, we built an 8-mm-period undulator sample consisting of 10 poles. Half of the poles were made of VP, and the other half were made of Dy. The sample was then installed in a vacuum chamber and mounted on a copper support, which was connected to a Gifford-McMahon refrigerator. This setup can cool the sample to around 50 K. The chamber was also equipped with a two-axis linear stage for actuating a magnetic sensor, which can measure the magnetic distribution. Figure 1 shows the measured magnetic distribution at a temperature of 53 K, where the Arabic and Roman numbers indicate the positions of VP and Dy poles, respectively. The peak fields of Dy poles were approximately 20% higher than those of VP poles, indicating the potential of Dy as a pole-piece material for cryogenic undulators.
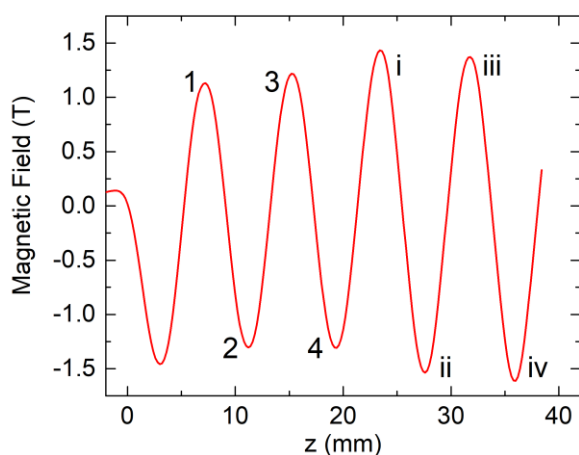
Fig. 1. Experimental demonstration of monocrystalline Dy as a pole-piece material for cryogenic undulators.

1-2. Front-end

(1) High-heat-load handling techniques

As part of an investigation of the thermal limitation of GlidCop made by a new manufacturing process, repeated irradiation tests with an electron beam irradiation system showed that the material failed at a much earlier stage than the predicted one based on the conventional Manson-Coffin equation. GlidCop made by the previous process followed the Manson-Coffin equation. To explore the origin of this fracture mode, the fatigue initiation point was examined using load-controlled fatigue tests and subsequent observations of the fracture surface. We noticed that fatigue crack propagation of GlidCop made by the new process must be evaluated using the stress intensity factor assuming that cracks and defects are present in the material.

(2) X-ray beam position monitor (XBPM)

Research to minimize the impact of changing the filling pattern on the XBPM output value continued in FY2019. Widening the insertion-device gaps at the fixed-point observation and increasing the applied voltage to the charge collecting electrodes reduced the deviation of XBPM readouts to less than a few μm RMS. However, further improvements require structural modifications to mitigate the space charge effect, which influences the change in the filling pattern. Therefore, we designed and fabricated a new inclined XBPM with the blade detector and an inclination of 1/60 of the photon beam axis direction. The new XBPM reduced the effect of changing the filling pattern to less than 1–2 μm.

(3) New beam profile monitoring system for X-ray beam exiting from the front-end

To develop a direct measurement method of the photon beam axis exiting from the front-end, a system to visualize the scattered X-rays from a chemical-vapor-deposition diamond thin film was installed at BL13XU [1]. Using a CCD camera with an energy resolution (PI-LCX LN, Princeton Instruments) as a detector, the fundamental radiation, which depends on the undulator gap, was selectively measured. Based on this result, we designed a dedicated chamber with an ideal detector arrangement to minimize the energy shifts of Compton scattering and elastic scattering. The chamber was installed at BL05XU. Similar to the case of BL13XU, the CCD camera can successfully visualize the photon beam axis.

2. Optics and transport channel

(1) Improvements in the stability of beam intensity and position (BL10XU)

BL10XU had two kinds of beam instabilities. The beam intensity fluctuated roughly with a daily periodicity. Each morning the beamline optical elements were adjusted, but the Bragg rotation angle of the first crystal ($\Delta\theta 1$) in the double-crystal monochromator (DCM) shifted and by the night, the

beam intensity lessened. However, the angle returned to the initial position the next morning. This shift was attributed to heat generation of the $\Delta\theta1$ motor. The $\Delta\theta1$ scan program prepared for users had the opposite backlash to the beamline control software. The double operation of the backlashes lengthened the driving time of the motor to approximately one hour. Consequently, the motor generated excessive heat. The heat was gradually translated into the stage components, which generated the instability. The periodicity was attributed to the daily routine of the adjustment. In addition to correcting the backlash setting, the $\Delta\theta1$ scan with a piezo-electric element was introduced.

The second instability was the beam position oscillated on an annual basis. It was first noted in June 2016, which coincided with a change in the feedback parameters of the storage ring operation. In 2019B, the original parameters were restored, and the oscillation has not been observed since. The cause was most likely seasonal changes in temperature. The light source section of this beamline is susceptible to the atmospheric temperature because the section is above the accessway to the inside of the storage ring. The feedback parameters set in June 2016 were assumed to be too sensitive.

(2) Study of the beam instability (BL35XU)

Frequently, the x-ray intensity at the sample position suddenly decreased at BL35XU, although none of the beamline equipment was moved. Monitoring the temperatures along the beam path revealed that the temperature of the first crystal holder in the DCM suddenly rose by 0.4 K, maintained this higher temperature for several hours, and then returned to the original temperature. During these temperature changes, the liquid

nitrogen for crystal cooling stably flowed with a constant temperature, flow rate, and pressure. If the rising originated from the increase in the heat load, the additional power would be estimated to be 27 W. However, the XBPM data suggested that the incident beam position and intensity were unrelated to the instability. Hence, further investigation in FY2020 is necessary.

(3) Adjustment of the optical axis (BL40B2)

At BL40B2, the incident white beam from the storage ring was emitted downward with an angle of 0.1 mrad. The beam deviated by 3 mm from the center of the incident slit (TC slit 1), placed at 30 m from the light source. Since the beam was not led to the experimental hutch at 60 m in the usual operation of optical elements, the BL staff raised the beam position by 6 mm by enlarging the crystal gap in the DCM. Accordingly, the optical elements after the DCM were adjusted to the off-position and slanted beam. To rectify this, in March 2020, the beam angle was corrected by changing the trajectory of the storage ring, and all the optical elements were realigned.

(4) Development of new liquid-nitrogen circulators for high heat load optics

Figure 2 shows prototypes of liquid-nitrogen circulators, which were fabricated and tested for cryogenic cooling of monochromator crystals as part of the SPring-8 upgrades. The new system was designed to not only manage a high heat load with low power consumption but also realize easy operations.

Fig. 2. New liquid-nitrogen circulators for high heat load optics.

In this design, the liquid-nitrogen coolant for the monochromator is confined in the closed loop that is comprised of a reservoir tank, a pump, a heat exchanger, and transport pipes. The reservoir tank has an electric heater to control the base pressure. The heated coolant is cooled in a coiled pipe immersed in a liquid-nitrogen bath. The liquid nitrogen in the bath is supplied externally and emitted as a gas. We experimentally demonstrated that a cooling power of 700 W could be managed stably, and are continuing studies to realize fully automated operations.

(5) New focusing mirror for soft X-ray micro-ARPES (BL25SU)

A monolithic Wolter type-I mirror was designed to provide a blight and stable sub-micron probe for soft X-ray micro angle-resolved photoemission spectroscopy (ARPES). The focusing mirror has ellipsoid and hyperboloid surfaces fabricated on a substrate. Due to the small comatic aberration and the single optical element, the system has a large tolerance for focus alignment. This Wolter mirror is designed to have large acceptance, achromatism, long working distance, high demagnification, and small comatic aberration. The mirror is suitable for ARPES experiments.

The new focusing system using the monolithic Wolter mirror was installed in an ARPES apparatus at BL25SU (Fig. 3). For typical conditions in APRES applications, the focusing sizes at the sample position are 0.4 µm in the vertical direction and 4 µm in the horizontal direction (Fig. 4). In FY2019, it was confirmed that it has a high tolerance to the alignment error due to the small comatic aberration.

Fig. 3. Soft X-ray micro-ARPES apparatus and installed monolithic Wolter mirror at BL25SU.
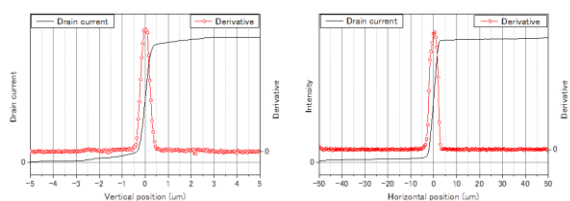

Fig. 4. Intensity profile (black line) and differentiation (red circles) measured using a knife-edge scanner in the vertical direction (left) and horizontal direction (right) at 750 eV.

(6) Removal of the front-end Be window to improve X-ray beam image (BL29XU)

The recent improvement in the stabilization of a cryogenically cooled monochromator revealed beam image degradation. Horizontal fringes were observed at experimental hutch 1 (EH1) (Fig. 5, left). The degradation was caused by the front-end (FE) Be windows. Although the Be of IF-1 grade was mirror-polished, a lot-to-lot uniformity was observed. The FE Be windows were removed to improve the beam image. To protect the ultrahigh vacuum of FE from vacuum failure of TC, all of the turbomolecular pumps in the optics hutch of BL29XU were replaced by ion pumps. Additionally, the fast-closing valve and differential pumping system were substituted for FE Be windows. Figure 5 shows beam images observed at EH1 before and after removal of the Be windows. The removal of the Be windows reduced the unevenness of the beam intensity observed as a horizontal stripe pattern.
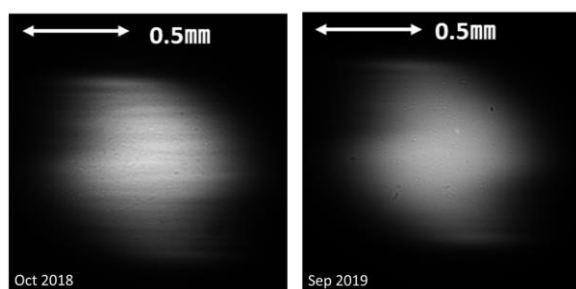
Fig. 5. Beam image measured with FE Be windows (left) and windowless (right) after DCM of BL29XU.

3. Radiation shielding for SPring-8 beamline

(1) Radiation shielding hutches

(1) -1　The barrier-free doors

To reduce the damage to experimental equipment while moving it in and out of the hutches, the automatic doors of the experimental hutches were replaced with barrier-free doors at BL19LXU.

(1) -2　A new type cable duct

A cable duct cover that can be opened and closed without hand tools and has a new locking mechanism to prevent erroneous operation is installed on an experimental hutch.

(2) Radiation-shielding calculations for the applications to the authority

The 46th change permission application contained radiation-dose calculations for the upper power revision, change of the movable gamma stopper to the synchrotron-radiation beamline shutter, structural changes of the synchrotron-radiation beamline shutter, and the penetration part in the ratchet of BL05XU.

(3) Radiation leakage inspection at beamlines

The following beamlines were inspected: BL45XU (upper power revision), BL04B1 (exchange of MBS), BL03XU (movement of DSS), BL13XU, BL29XU, BL 37XU, and BL 41XU (reinstallation of the local shield), BL05XU (46th change permission), BL19LXU (barrier-free door), and BL28XU (movement of beam pipe).

(4) Radiation measurements and method development

The HD-V2 and EBT3 GafChromic films were irradiated with ^{60}Co gamma rays to calibrate and update the dose conversion factors from the optical density in the GafChromic film-reading equipment. To investigate the radiation tolerance of LED light, GafChromic films were used for the dose measurement.

4. Beamlines of SACLA

4-1. XFEL beamlines

In FY2019, an important milestone for the upgrade

of SPring-8 was achieved. The two XFEL beamlines (BL2 and BL3) were operated in parallel to produce hard X-ray pulses in the range of 4–20 keV [2]. The main linac of SACLA drives the two beamlines by switching the electron-beam route in a pulse-by-pulse manner. The switching operation was further developed for beam injection into the storage ring of SPring-8. This new injection scheme was applied to simultaneous user operations of SACLA and SPring-8.

The X-ray transport channels and experimental hutches (EHs) were also upgraded. A new beam shutter (DSS2) was installed to BL3 at the downstream end of EH1 (Fig. 6). This shutter can operate independently from the existing shutter (DSS1), which is located in the optics hutch (OH2). DSS2 enables continuous monitoring of XFEL pulses using the photon diagnostic systems at EH1. The presence of two diagnostic systems is especially important to keep the XFEL beam in a stable condition. One serves as an arrival timing monitor, which measures time intervals between pulses of XFEL and the synchronized optical laser [3]. The other is a single-shot spectrometer to measure the spectrum of each XFEL pulse [4]. Due to DSS2, these two monitors can work continuously during user experiments even while users or staff are working in the downstream hutches. Continuous monitoring is important to perform experiments efficiently in a stable XFEL beam condition.
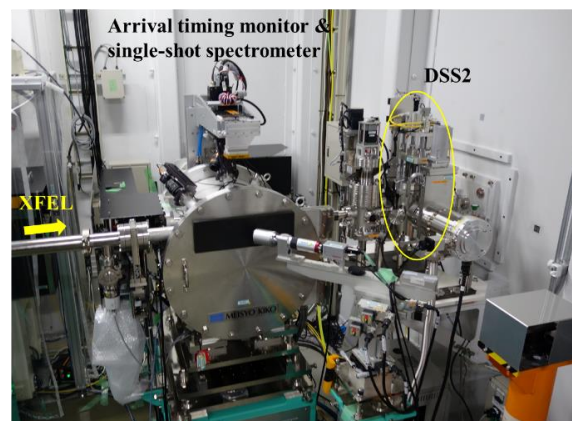

Fig. 6. XFEL diagnostic systems and DSS2 in EH1 of SACLA BL3.

4-2. Soft X-ray FEL beamline

The soft X-ray (SX) FEL beamline (BL1) is driven by a dedicated 800-MeV linac (SCSS+) to produce SX pulses with photon energies between 40 eV and 150 eV, and a pulse width of ~30 fs [5, 6]. However, the magnets of the undulator degraded because the length of each undulator unit (5 m) was too long for the 800-MeV electron beam. In FY2020, the undulator line will be laterally shifted by 5 mm to mitigate the effect of the magnet degradation.

New experimental instruments were developed under the SACLA Basic Development Program and the SACLA Research Support Program for Graduate Students (e.g., ellipsometer for magneto-optical Kerr effect measurement [7,8] and sub-micrometer focusing optics for SX-FEL [9]). These instruments were used to visualize the magnetic structures of samples with a resolution of 7 μm [10]. For more advanced focusing systems with two-stage optics, a branch line was built in the section of the SX transport channel (Fig. 7).
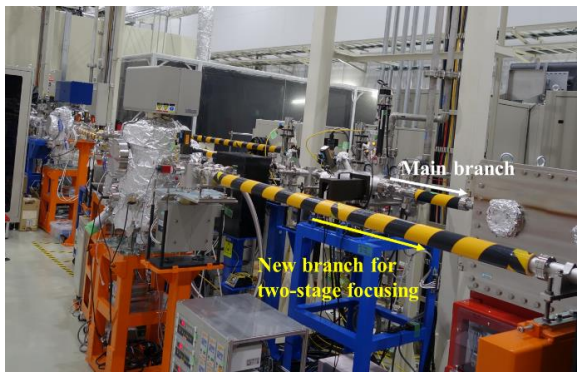
Fig. 7. Branched beamline for two-stage focusing of SX-FEL at SACLA BL1.

Takashi Tanaka[*1], Sunao Takahashi[*1], Yasunori Senba[*1], Hiroshi Yamazaki[*1], Haruhiko Ohashi[*1], Kunikazu Takeshita[*1], Nobuteru Nariyama[*1], Shunji Goto[*1], Yuichi Inubushi[*2], Shigeki Owada[*2], Kensuke Tono[*2], and Makina Yabashi[*3]

[*1] Light source division, JASRI

[*2] XFEL Utilization Division, JASRI

[*3] XFEL Research and Development Division, RIKEN SPring-8 Center

References:

[1] T. Kudo et al., *Review of Scientific Instruments* **91**, 033103 (2020)

[2] K. Tono et al, *J. Synchrotron Rad.* **26**, 595-602 (2019).

[3] T. Katayama, et al., *Struct. Dyn.* **3**, 034301 (2016).

[4] Y. Inubushi, et al., *Phys. Rev. Lett.* **109**, 144801 (2012).

[5] S. Owada, et al., *J. Synchrotron Rad*. **25**, 282-288 (2018).

[6] S. Owada et al., *J. Synchrotron Rad*. **27**, 1362-1365 (2020).

[7] M. Araki et al., *e-JSSNT* **18**, 231-234 (2020).

[8] K. Yamamoto et al., *Appl. Phys. Lett.* **116**, 172406 (2020).

[9] H. Motoyama et al., *J. Synchrotron Rad.* **26**, 1406-1411 (2019).

[10] Y. Kubota et al., *Appl. Phys. Lett*. **117**, 042405 (2020).